Supplementary Information Inventory:

Supplemental Information For "LIS1 and NudE Induce a Persistent Dynein Force-Producing State" by McKenney et al.

Supplementary Information Inventory:

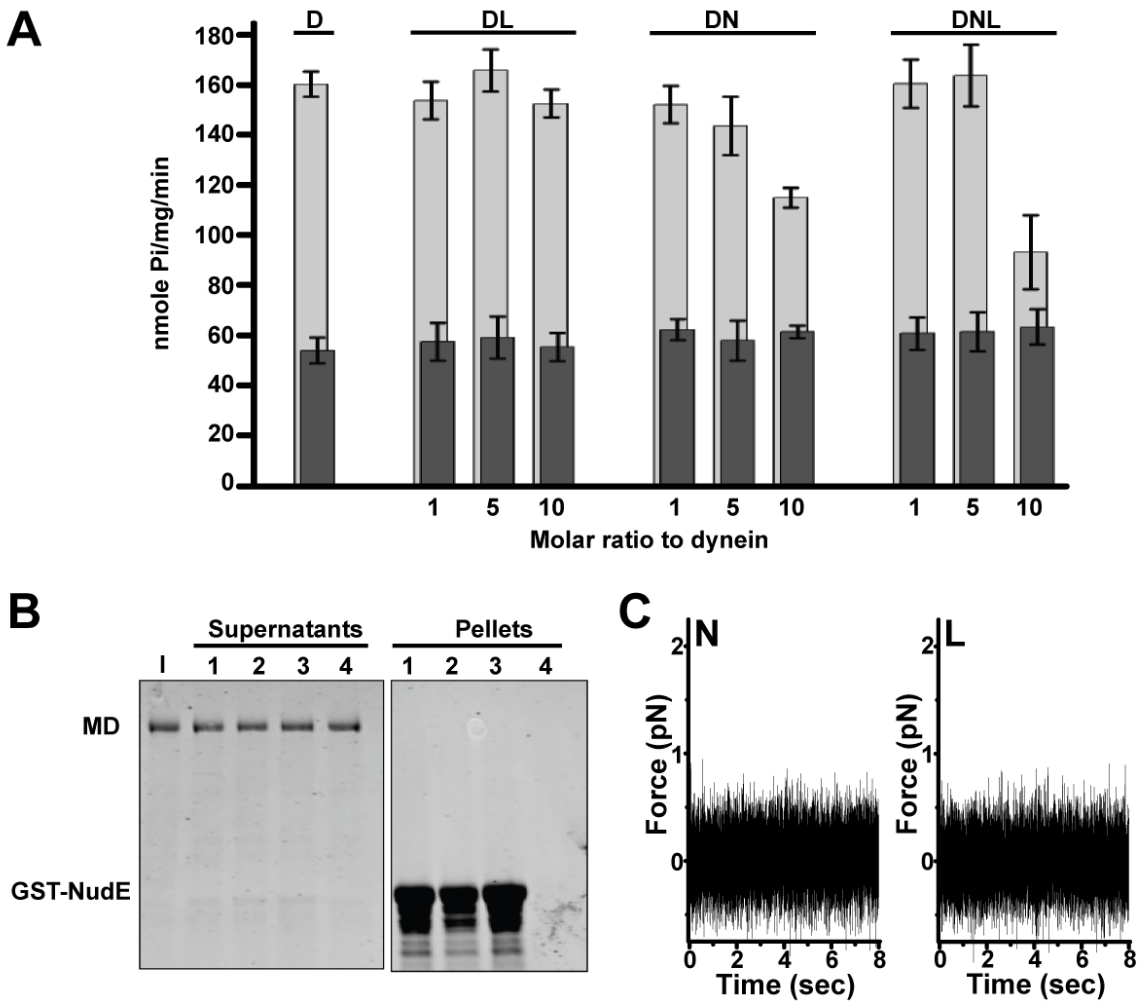

Fig. S1, relates to Fig. 2. Effects of NudE and LIS1 on microtubule binding and ATPase activity. **(A)** Brain cytoplasmic dynein (D) was mixed with NudE (DN) and/or LIS1 (DL or DNL) with (light grey bars) or without microtubules (dark gray bars), and ATPase activity was determined. LIS1 and NudE had no effect on basal ATPase activity, but NudE alone and NudE plus LIS1 inhibited the microtubule-stimulated ATPase component. Error bars indicate standard deviation from 3 independent experiments. **(B)** Pull-down of purified dynein motor domain with GST-tagged NudE as a function of nucleotide composition. No interaction was observed under conditions of no nucleotide (lane 1), ATP (lane 2) or ATP + VO_4 (lane 3). Input (I) and control beads (lane 4) are

shown. **(C)** NudE and LIS1 do not bind microtubules in the absence of dynein. Beads incubated with NudE alone (N), and LIS1 alone (L) were situated next to a microtubule in an optical trap and their position monitored. Systematic displacements of beads from the center of the trap (zero in all plots) would reveal individual motor events. Such events are non-existent for (N) and (L). Non-specific binding events should also be detectable in this assay, as evidenced by decreased noise in bead tracings in the absence of any systematic displacement of the beads. Such changes were not observed for N and L beads, arguing against non-specific bead-MT binding. Moreover, these beads quickly diffused from the microtubules once the trap was turned off, further confirming the lack of any MT-binding activity in those assays.

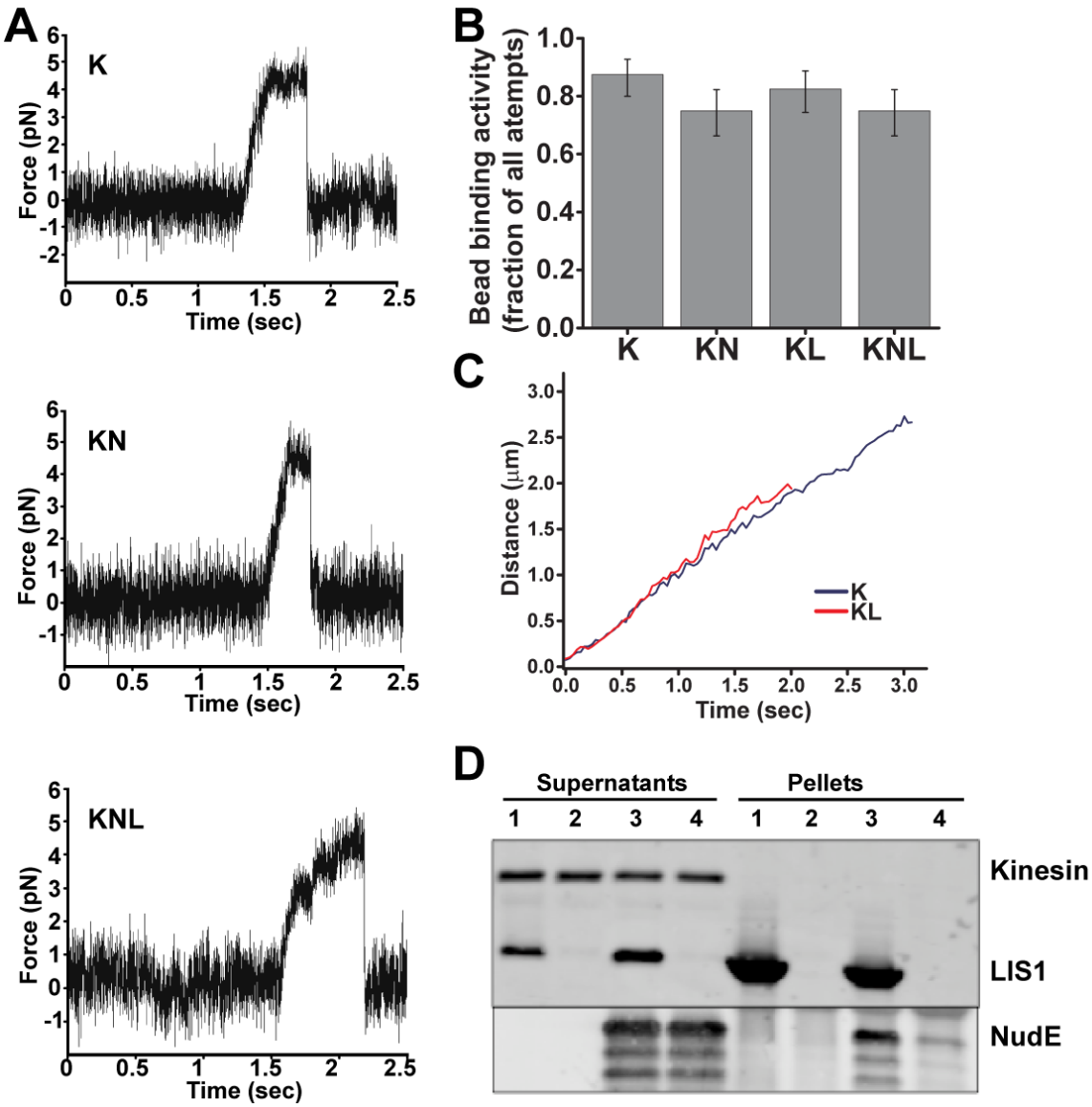

Fig. S2, relates to Fig. 3. **Lack of effect of NudE and LIS1 on kinesin motility and force production. (A)** Representative records of single motor force production in an optical trap are shown for beads adsorbed with a recombinant K560 kinesin construct alone (K), in the presence of NudE (KN; K:N 1:10), and in the presence of both NudE and LIS1 (KNL; K:N:L 1:10:10). Kinesin force production and stalling behavior under load were unaffected by LIS1 and NudE. **(B)** Kinesin bead binding to MTs was minimally affected by the presence of NudE, LIS1, or both NudE and LIS1 (n = 40 in all

cases, exact CI error bars are reported). **(C)** Traces of processive motion along MTs for beads driven by kinesin alone (blue) and kinesin in the presence of 3X molar excess of LIS1 (red) reveal no pauses in motion. This is in contrast to frequent pauses seen for dynein motility in the presence of comparable levels of LIS1 (Fig. 2B). **(D)** Purified, recombinant kinesin (K560) does not interact with LIS1 (lane 1) or a LIS1-NudE complex (lane 3). No LIS1, NudE or Kinesin was pulled down by beads lacking LIS1 antibodies (lanes 2, 4).

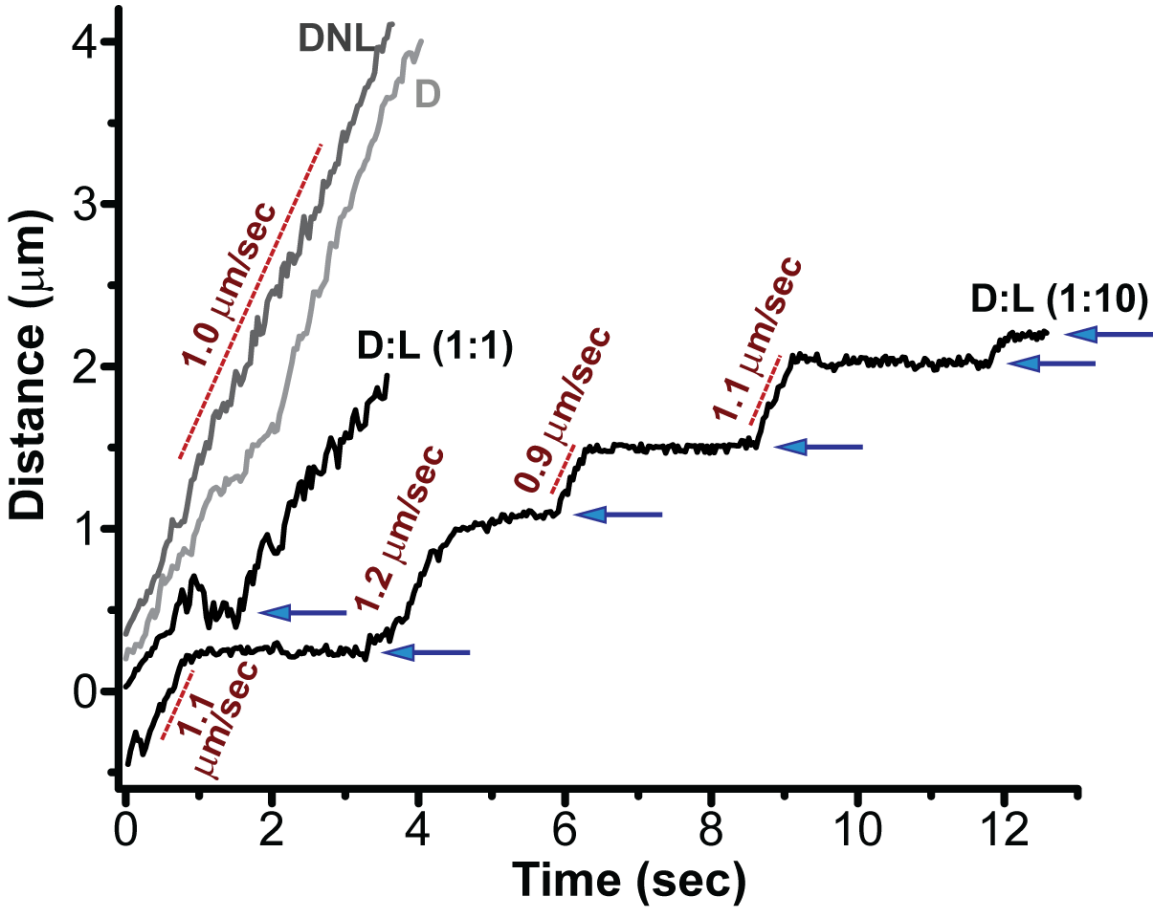

Fig. S3, relates to Fig. 3. Additional examples of D, DL, and DNL motility.

Individual traces of motor-driven movements along microtubules (molar ratios were D:L=1:10 and D:N:L = 1:9:10)**.** DL bead movement is interrupted by unusually clear and frequent pauses (blue arrows), while D and DNL bead movement is prolonged and continuous.

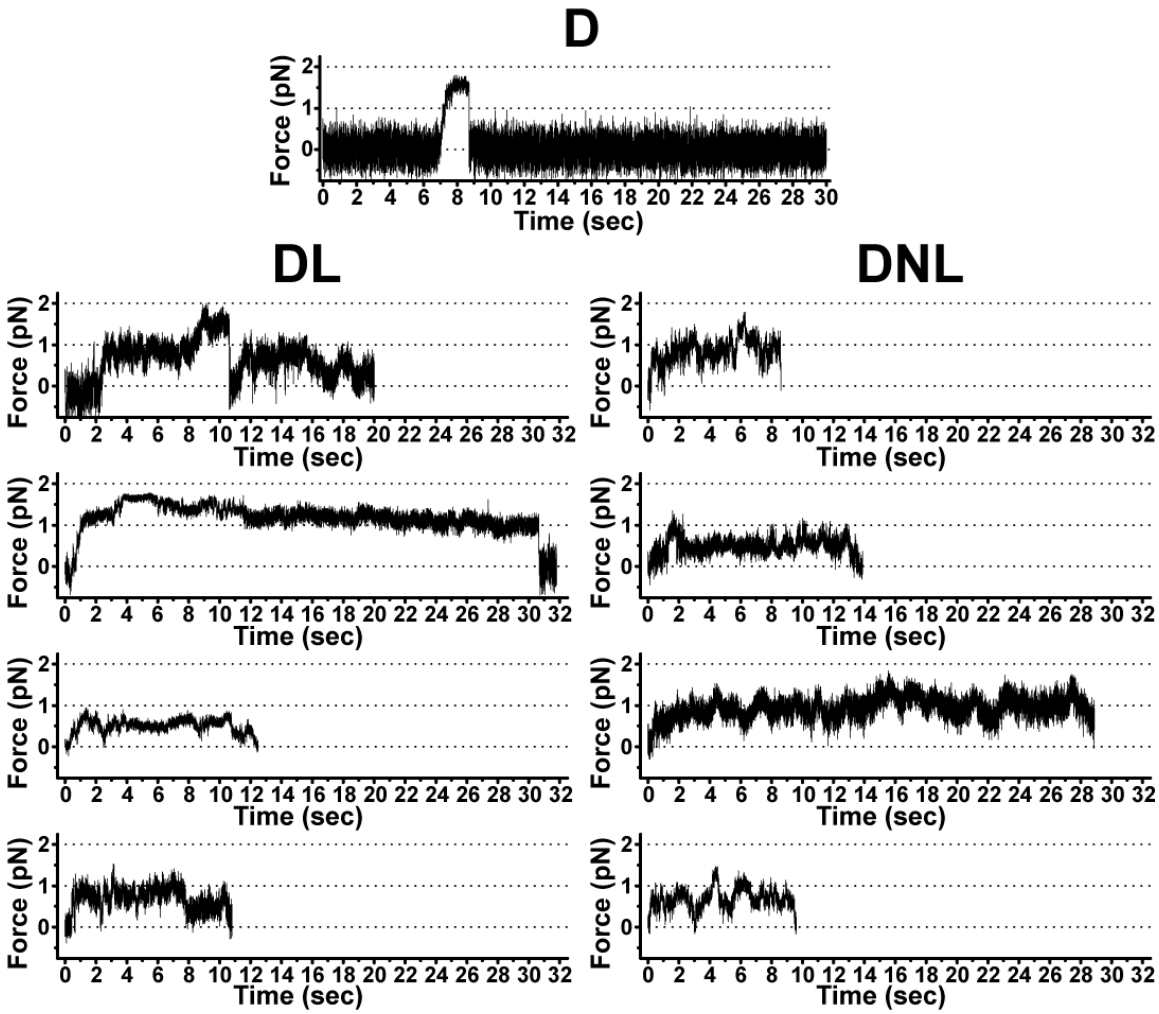

Fig. S4, relates to Fig. 4. Additional examples of LIS1 and NudE effects on dynein force production. Trace of dynein bead position in optical trap (D) is shown at top, including a longer force-producing event (~2 sec), which is rare for dynein alone. Traces of dynein bead position are shown below in the presence of LIS1 (DL;1:10 D:L) or NudE plus LIS1 (DNL; 1:9:10 D:N:L; right panels) showing commonly observed persistent force events.

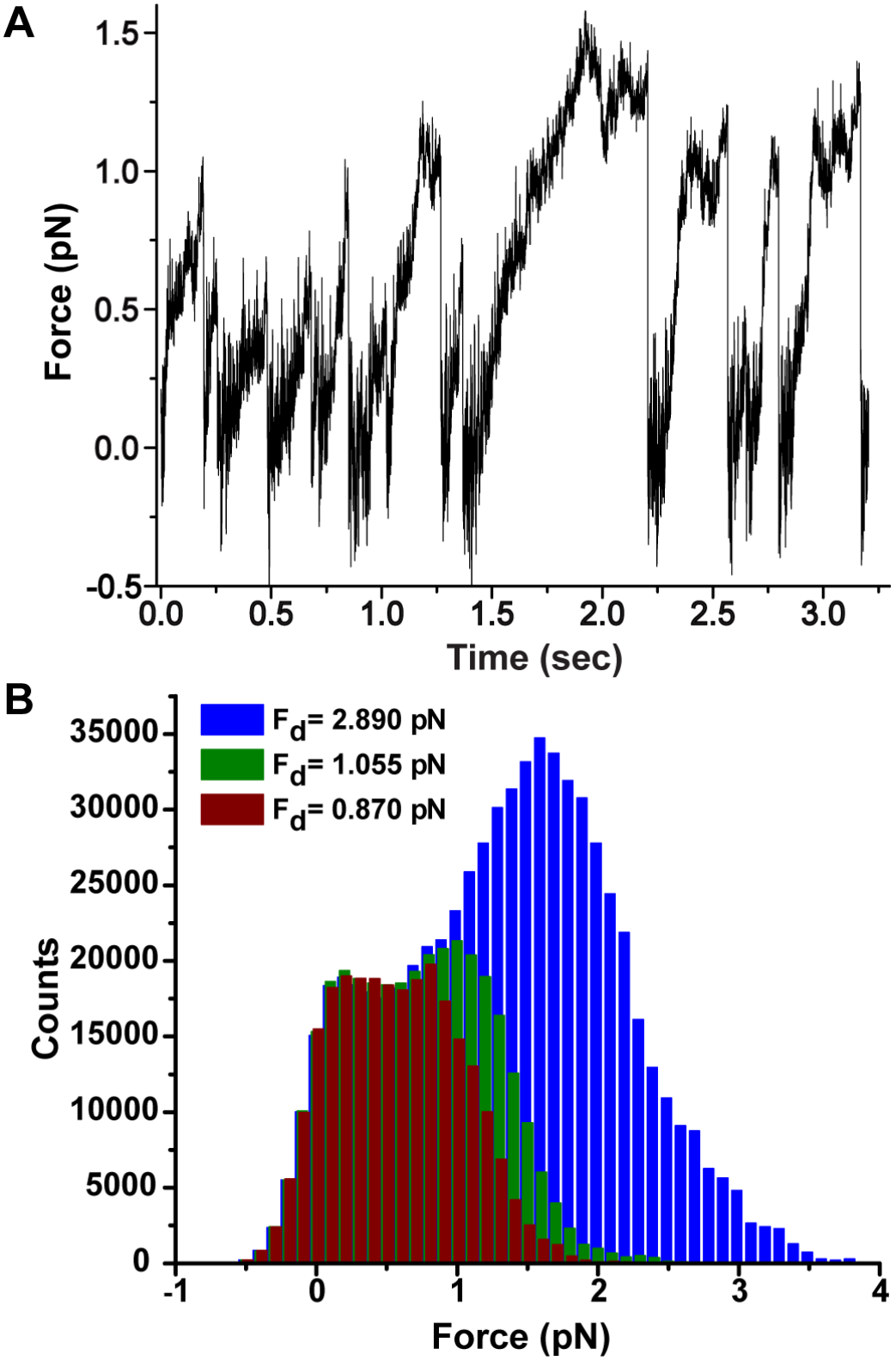

Fig. S5, relates to Fig. 6. ***In silico*** **modeling of single and multiple dynein activity**.

(A) The model implemented in this paper is necessarily crude since many key parameters of cytoplasmic dynein function are not known. However, the model does capture important known observables, such as unloaded velocity, overall force production scale, and propensity to move bi-directionally rather than cleanly stall under load. **(B)** We simulated motility of a cargo driven against a trap by a maximum of 2 motors (N=2). The effect of the addition of NudE and LIS1 was modeled to decrease the detachment rate of the motors under load, such that at 2 pN the detachment time increased by 50% (and 500% for LIS1 alone), as suggested by the superforce experiments (Fig 5). This was implemented by varying detachment scale F_d such that an increase of F_d resulted in a corresponding increase for time to detachment under load (see Supplementary Information, section "Theoretical model for dynein-based motility"). The histograms of all predicted bead positions thus obtained (trap stiffness of 0.01 pN/nm) were calculated for 1000 simulations for baseline case, as well as 50% and 500% increase in time to detachment at 2 pN load (F_d of 0.87 pN (red), 1.055 pN (green), and 2.89 pN (blue) respectively). The predicted robust shift to higher values of force for the lower detachment rate case demonstrates that this parameter can have strong effect on multiple motor performance. Notice also that the number of total counts rises as the detachment rate falls, directly implying that reduced detachment rate significantly enhances ensemble's ability to withstand load.

Extended Experimental Procedures

ATPase Assays: ATPase activity was assayed using the malachite green method (Hook et al., 2005) in Tris-KCl buffer (Paschal et al., 1987) and incubated at 37^{o}C for 15 minutes in the presence of 1mM ATP. For microtubule stimulation, taxol-stabilized microtubules were added to 1mg/mL final concentration before the addition of ATP.

Immunoprecipitations: Immunoprecipitations in Fig. 1B were performed similarly in Tris-KCL buffer (20mM Tris pH 7.6, 50mM KCl, 5mM $MgSO_4$, 0.5mM EDTA) except the purified LIS1 protein was immobilized onto Protein A beads (Invitrogen) using an anti-N-terminal LIS1 antibody (Faulkner et al., 2000).

Sucrose Density Gradient: For sucrose gradient analysis, purified dynein motor domain (800nM) with or without purified LIS1 (1600nM) and the indicated nucleotides were mixed together on ice for 1 hour. The mixture was loaded onto 11mL linear 5-20% sucrose density gradients in buffer (35mM PIPES pH 7.2, 5mM $MgSO_4$, 1mM EDTA, 0.5mM EGTA) containing the corresponding nucleotides and centrifuged at 32K rpm for 16 hours in a Beckman SW41Ti rotor. Fractions (800uL) were collected and analyzed by gel electrophoresis and Coomassie brilliant blue staining.

Bead Assays: Bead assays were performed as previously described (Mallik et al., 2004), except that GTP and taxol were omitted from the assay buffer, and an oxygen scavenging system was used as previously described (Vershinin et al., 2007). Video recording and analysis of bead motion were performed as previously described (Carter et al., 2005; Vershinin et al., 2007). Force measurements were also carried out as previously described (Vershinin et al., 2007). The majority of assays were done at motor/bead incubation

ratios such that 30% or fewer beads showed MT-binding activity (Vershinin et al., 2007), so that the function of single dynein motors was characterized.

Protein adsorption on beads was done via sequential incubations (10 minutes at room temperature). Dynein was first incubated with carboxylated polystyrene beads (Vershinin et al., 2007), and the beads were then washed via mild centrifugation and re-suspended in casein-containing buffer. In assays intended to study complexes, we followed this preparation with one of two approaches (referred to in the main text as "washed" and "unwashed" assays). In the "washed" assays, after preparing the dynein-beads, each additional protein (NudE and/or LIS1) was incubated with the beads, and each incubation was followed by mild centrifugation to remove the unattached component from solution. (Assays without such intermediate buffer exchanges were found to give similar results). After all such incubations, a final wash was performed. This was then followed by re-suspension in the assay buffer described above. The "unwashed" assays were prepared similarly, however the components were not removed via centrifugation following incubations. In the experiments described here, the incubation order was Dynein then NudE for DN assays, Dynein then LIS1 for DL assays and Dynein then NudE then LIS1 for DNL assays.

We have also attached dynein to polystyrene beads via the 74.1 monoclonal Anti-DIC antibody (Millipore Bioscience Research Reagents, Temecula, CA). In these assays, the mAb was first non-specifically adsorbed on beads (~1:20 bead:antibody molar ratio at incubation). Upon incubation, the beads were pelleted via mild centrifugation and then

resuspended in 5 mg/mL casein buffer. Upon incubation the beads were again pelleted via mild centrifugation and then resuspended and incubated in motility buffer containing dynein.

Multiple motor escape experiments. To test the effect of NudE and LIS1 on multiple dynein motors, we devised a new type of trap escape experiment. For a given dynein concentration, we first attached dynein to beads, and blocked the beads with casein. An examination of force production records for beads held near a microtubule in an optical trap allowed us to determine the approximate motor number and to choose a laser power such that only a small fraction of the control dynein beads were able to exert enough force over a long enough period of time (sufficient to observe several prominent events; 30 sec typical) to escape from the trap. Once the appropriate trap stiffness was set for a particular dynein concentration, we then performed parallel experiments on beads in the presence or absence of NudE and LIS1 and determined the fraction of beads to escape the trap. Two different dynein concentrations were used to change the mean number of engaged motors, and correspondingly we used two different trap stiffness conditions, 0.01 pN/nm and 0.02 pN/nm for the low and high dynein concentrations, respectively (maximum trap force ~ 1.8 and 3.7 pN).

Binding frequency analysis from quadrant photodiode records. To compare binding frequency in dynein-only and dynein/NudE assays using the force production recordings (Fig. 3a,b), we faced the limitation that the extremely short processivity of the dynein/NudE complex made it difficult to distinguish between bead motion due to motor

activity and bead motion due to thermal noise. To address this difficulty, we developed the following data analysis algorithm:

1. Data was median filtered using a 10 point window (5 ms), to eliminate spurious noise.
2. Filtered data was normalized by the maximum displacement occurring in each record.
3. The start of each binding event was determined to occur when the instantaneous bead displacement first exceeded a defined constant threshold.
4. The end of each binding event was determined to occur when the instantaneous bead position decreased, so that it was within 2 standard deviations of the trap center, where the standard deviation refers to the extent of thermal noise and was extracted from each record.
5. Once the record had been processed, and all the binding events identified, we counted the number of binding events and normalized this number by the time duration of each record, to extract the binding rate.

The normalization (rescaling) in Step 2 was done so that the differences in bead travel between assays would not affect the binding frequency analysis. Note however, that this rescaling effectively amplifies noise for low-travel assays such as our dynein/NudE assay, so that in these assays noise-driven displacements are more likely to be improperly scored as binding events. Therefore, the estimate of binding reduction due to NudE provides a lower bound, and so the actual reduction is likely to be stronger.

Classifying different types of binding. From observing beads in the dynein-NudE assays, we realized there were significantly more binding and release events (with

negligible actual travel) than there were actual bead displacements appearing to reflect motor-driven transport. We were interested in quantifying the number of both classes of events. The first class provided evidence that at least one motor was present and marginally functional on the bead. The second class is the events that, though short and rare, reflect clearly processive transport. The analysis above using the quadrant photodiode was both very sensitive and with very high temporal resolution, and thus able to identify both classes of events. In addition, however, we wanted to focus only on the second class of events. To do this, we used our video records of bead movements in the optical trap. This system predominantly did not "see" the first class of events, because the data rate for video recording (NTSC: ~33 ms/frame) did not resolve fast events whose travel fell below ~50-60 nm, the level of thermal-driven positional noise. Thus, binding events identified from video records (as opposed to quadrant photo-diode records) reflected significant motor activity. We therefore used video identification of microtubule binding as a metric for looking at significant events (Fig. 4c).

Superstall experiments. A bead driven by a single dynein motor was allowed to move 100 nm from the center of a weak optical trap (k = 0.01 pN/nm). At this displacement, the motor was still not subjected to stall conditions. The position of the bead was evaluated in a sliding 10 msec window to reduce noise. Once the smoothed bead position exceeded 100 nm, the trap stiffness was automatically doubled via a custom software control system, and the motor was subjected to ~2 pN of force (the 10 msec smoothing window may have resulted in a slight uncertainty of the initial instantaneous superforce). Both bead position and laser power were simultaneously recorded so that the onset of

superforce regime could be determined in subsequent analysis. The superstall event started when the laser power was increased (T=0), and ended when the motor detached from the microtubule, identified as the time when the bead displacement from trap center fell to within thermal noise level (typically, a sharp drop in bead position). Custom Matlab (Mathworks, Natick, MA) and LabView (National Instruments, Austin, TX) software were used for data recording and analysis.

Theoretical model for dynein-based motility:

We assume that the dependence of the velocity *V* on applied load F can be well approximated for a single dynein motor by the following relation:

$$v(F) = v\left(1 - \left(\frac{F}{F_S}\right)^w\right) \tag{1}$$

where v is the unloaded velocity of dynein motor, F is the applied force, and F_s is the stall force. We chose w=0.25 to model predicted sub- linear force-velocity relationship of dynein motor (Singh et al., 2005). Other force-velocity relationships including super-linear ones were investigated (results not shown) and were found to produce qualitatively similar results (enhancement of multiple motor ensemble performance under load).

For motor's step size d, load-dependent rate of forward stepping is given by

$$k_{Step}(F) = \begin{cases} \frac{v}{d}\left(1 - \left(\frac{F}{F_S}\right)^w\right) & F \le F_S \\ 0 & F > F_S \end{cases} \tag{2}$$

A forward load is assumed to not alter the motor cycle, so F = 0 for forward loads in Eqn. 2.

Following (Klumpp and Lipowsky, 2005), we use the Kramers's theory formula for the rate of motor detachment under backward load F

$$\varepsilon(F)=\varepsilon\exp\left(\frac{F}{F_d}\right) \tag{3}$$

and we assume similar dynamics for back-stepping probability of dynein

$$k_{Step}(F)=\frac{v}{Bd}\exp\left(\frac{F}{F_d}\right) \tag{4}$$

where the scaling factor B is set to assure that the probability of back-stepping under no load is small relative to the probability of forward-stepping (here B=40 which translates into a 2.5% rate of back-stepping under no load).

In the presence of the viscous load, position of the cargo is determined by the external load applied by the trap, forces exerted by motors on the bead as well as thermal noise. If a spherical bead of radius r immersed in a medium of dynamic viscosity η were subject to a net force *f* then (per Stokes' law) this would cause the bead to move with velocity $v_{drift}=(f/6\pi\eta r)$. Note that our simulations use the effective viscosity of water near the surface which is higher than bulk viscosity as per Faxen's law. Our simulations are not very sensitive to this scaling and similar qualitative results were seen for viscosities between 1e-3 $N\ s/m^2$ and 3e-3 $N\ s/m^2$.

To calculate the net motion of the bead over time interval Δt we superimpose the deterministic drift $x_{drift}=v_{drift}.\Delta t=(f/6\pi\eta r)\Delta t$ on the Brownian displacements x_{random} which are modeled as a random variable drawn from a normal distribution with mean square displacement $2D\Delta t$ (Beausang et al., 2007; Kunwar et al., 2008; Mogilner et al., 2002).

Here D is the diffusion constant of the bead (thermal displacements of the motors are assumed to be negligible).

To summarize, the bead displacement at time t and t+Δt are related by:

$$\vec{x}(t+\Delta t) = \vec{x}(t) + \vec{x}_{random} + \vec{x}_{drift} = \vec{x}(t) + \vec{x}_{random} + \frac{\vec{f}}{6\pi\eta \mathrm{r}}(\Delta t) \quad (5)$$

The net force f on the bead is given by

$$\vec{f} = \vec{F} + \sum_{i=1}^{n} f_i$$

where F is the external force on the bead whose magnitude depends on the displacement of the bead from the trap center $F=k_{trap}(x-x_{trap})$. Note that an engaged dynein motor forms a linkage between the cargo and the microtubule with rest length 50 nm and stiffness 0.32 pN/nm. In our model, the i^{th} motor exerts a restoring force $f_i = k\Delta l_i$ when it is stretched by Δl_i beyond their rest length and have no compressional rigidity, i.e. they exert no force when compressed.

Simulation algorithm

For each time step, we visit each of the N motors and determine their tentative states (attached or detached) and positions. If a motor is currently unattached, we give it a chance to attach with a probability determined by the assumed "on-rate" (P_{on}). If a motor is currently attached, there are four possibilities: it can remain stationary, take a forward step, take a backward step, or detach. To determine what the motor does, we first calculate the force it experiences taking into account that the force felt by a given motor depends on its position relative to the position of the bead. Once the load on a motor is

determined, we then test if it steps, remains stationary, or detaches, where the probability of each event is determined from the single motor model (see above). When we have determined the tentative states and positions of all N motors, we update the states and positions of all motors simultaneously. Finally, we calculate the new position of the bead using the new motor states and positions (Eqn. 5). We then record the positions and states of all motors and the overall location of the cargo.

In our simulations, a cargo carries N motors (which is the upper limit on the number of instantaneously engaged motors n). The update procedure for each configuration is detailed below.

Algorithm in detail: We denote the current position of the cargo by x, the current time by t, and the current number of engaged motors by n. To start with the initial condition of single motor attached, we place the bead's center of mass at the center of the trap x_{trap} on the track. The motor is allowed to attach to any discrete binding site on the track within distance l on either side of the bead's center of mass. Thus, at $t = 0$, $x = x_{trap}$ and $n = 1$. We update the state of the model in steps of Δt up to time t_{max}. Every motor is updated once and only once in a given time step.

For each time step, if t > tmax, then terminate further simulation, otherwise for each motor, we follow the update algorithm below:

(a) Update the motor state:

A1. *Updating a detached motor:* Examine every motor on the cargo. If a given motor is in a detached state, it gets an opportunity to attach with probability $P_{on} = \pi\Delta t$ to any binding site on the track within distance l on either side from the center of mass of the bead. The probability of binding to the track is modeled as a truncated Gaussian with width (HWHM) equal to half motor length (25 nm). We have also tested uniform binding probability model and seen qualitatively similar results.

A2. *Updating an attached motor*: Examine every motor on the cargo not already updated in step A1. If a given motor is engaged then:

B1. Test for detachment with probability given by Eqn. 3. If detachment occurs then go to step B3.

B2. Test for forward stepping with a probability given by Eqn.2 or back stepping with a probability given by Eqn.4. The test is designed to be mutually exclusive so that only one outcome can occur per time step. If a step occurs then x_i is incremented to $x_i + d$ for a forward step or $x_i - d$ for a backward step.

B3. Proceed to update the next motor or step (b) if all motors are updated.

(b) Calculate n (the number of instantaneously engaged motors): if n = 0, then record the final position of the bead $x_{final} = x$, and end the simulation, else update the cargo position as per Eqn. 4 and proceed to simulating the next time step.

Parameter Values for Simulations

The parameter values used are v=1 μm/s, d=8 nm, $\varepsilon = 1s^{-1}$, F_s=1.5 pN and F_d= 0.87 pN, 1.055 pN, and 2.89 pN as indicated, l=50 nm, k=0.01pN/nm (low number of motors in Fig. 6B) and 0.02 pN/nm nm (high number of motors in Fig. 6B), r=0.25 μm. In each case, Monte Carlo results were obtained from runs each having a duration of t_{max}=100 s (1 time step=10^{-7}s).

Our model assumes that all N motors are clustered at one spot on the cargo however in reality motors likely bind randomly on the surface of the bead. We expect that motors that bind away from the microtubule-facing spot on the bead will have lower on-rate and we have attempted to take such geometric factors of motor binding into account when modeling beads with high vs. low motor density (N=1,2, and 4). Thus, for low motor density we assumed $\pi = 0.4s^{-1}$ and for high motor density $\pi = 4s^{-1}$. The simulations shown in Fig. 6 for the low trap stiffness case had 20% of beads with N=2 and 80% with N=1. In the high trap stiffness case, N=4 was used for all beads.

For trap escape modeling in Fig 6B, each run was simulated as described above and then all runs (total runs=10000) were split into non-overlapping groups of 20 to account for the fact that in the *in vitro* experiments each bead was given multiple chances to escape from the trap (20 attempts typical). Failure of trap escape for each group was recorded if none of the runs in the group resulted in an escape.

Reporting error bars for binomial-distributed data

It is common to report standard error of the mean (or standard deviation) as an error bar estimate for Gaussian distributed variables. However, a binomial distribution is in many cases poorly approximated by a normal distribution. We have therefore used a conceptually similar error estimate: 68.2689% exact CI for a binomial distribution for all data which is expected to have a binomial distribution (Fig. 3B, 4D, 6B, and S2). A Bayesian estimation with uniform prior distribution yielded similar values.

Supplemental References

Beausang, J. F., Zurla, C., Finzi, L., Sullivan, L., and Nelson, P. C. (2007). Elementary simulation of tethered Brownian motion. Am J Phys *75*, 520-523.

Carter, B. C., Shubeita, G. T., and Gross, S. P. (2005). Tracking single particles: a user-friendly quantitative evaluation. Phys Biol *2*, 60-72.

Faulkner, N. E., Dujardin, D. L., Tai, C. Y., Vaughan, K. T., O'Connell, C. B., Wang, Y., and Vallee, R. B. (2000). A role for the lissencephaly gene LIS1 in mitosis and cytoplasmic dynein function. Nat Cell Biol *2*, 784-791.

Hook, P., Mikami, A., Shafer, B., Chait, B. T., Rosenfeld, S. S., and Vallee, R. B. (2005). Long range allosteric control of cytoplasmic dynein ATPase activity by the stalk and C-terminal domains. J Biol Chem *280*, 33045-33054.

Klumpp, S., and Lipowsky, R. (2005). Cooperative cargo transport by several molecular motors. Proc Natl Acad Sci U S A *102*, 17284-17289.

Kunwar, A., Vershinin, M., Xu, J., and Gross, S. P. (2008). Stepping, strain gating, and an unexpected force-velocity curve for multiple-motor-based transport. Curr Biol *18*, 1173-1183.

Mallik, R., Carter, B. C., Lex, S. A., King, S. J., and Gross, S. P. (2004). Cytoplasmic dynein functions as a gear in response to load. Nature *427*, 649-652.

Mogilner, A., Elston, T., Wang, H. Y., and Oster, G. (2002). Molecular motors: Theory. Joel Keizer's Computational Cell Biology, 321-355.

Paschal, B. M., Shpetner, H. S., and Vallee, R. B. (1987). MAP 1C is a microtubule-activated ATPase which translocates microtubules *in vitro* and has dynein-like properties. J Cell Biol *105*, 1273-1282.

Singh, M. P., Mallik, R., Gross, S. P., and Yu, C. C. (2005). Monte Carlo modeling of single-molecule cytoplasmic dynein. Proc Natl Acad Sci U S A *102*, 12059-12064.

Vershinin, M., Carter, B. C., Razafsky, D. S., King, S. J., and Gross, S. P. (2007). Multiple-motor based transport and its regulation by Tau. Proc Natl Acad Sci U S A *104*, 87-92.